SPE 87627

ESP Stages Air-Water Two-Phase Performance – Modeling and Experimental Data

Javier Duran, SPE, Ecopetrol, Mauricio Prado, SPE, The University of Tulsa.

Unsolicited 2003

Abstract

ESP performance is affected by the presence of free gas. Two-phase performance is sensitive to intake pressure, insitu gas fraction, flow rates, fluid properties, rotational speed, pump type, pump size and number of stages used. The degree of head deterioration varies from a simple reduction in performance to more severe problems such as surging and gas locking. So far, no comprehensive predictive method is available to predict the performance of centrifugal pumps or the problems of surging and gas locking under two-phase conditions.

The University of Tulsa Artificial Lift Projects is currently conducting experimental and theoretical research on the two-phase behavior of centrifugal pumps. In this work, an experimental and theoretical study was conducted as a continuation of Pessoa (2000) and Beltur (2003) work. The main contribution of the present study with respect to earlier experimental research is a complete mapping of the multiphase performance of one stage of a commercial ESP pump (series 513 with best efficiency point of 6100 bpd at 3500 rpm). The effects of gas and liquid rates and stage intake pressure when operating at 42Hz (2450 rpm) were investigated experimentally. Analysis of the experimental data enabled the development of models and correlations to predict the performance of ESP under two-phase flow conditions. A model was developed to predict the stage pressure increment under bubbly flow regime. A correlation was obtained to predict the stage pressure increment under elongated bubble flow regime. Also correlations were established for the determination of the flow pattern transition boundaries.

The application of this research will help in designing of proper pump for gassy wells applications. Prior knowledge of surging and gas lock conditions will help in defining safe operating conditions for the pump.

Introduction

Centrifugal pumps are dynamic single or multistage devices that use kinetic energy to increase pressure. Existing impeller and diffuser designs are very successful to handle low viscosity, single-phase incompressible fluids, but are severely impacted by free gas, highly compressible or viscous fluids.

When handling free gas, the centrifugal pump suffers performance degradation. In addition to performance degradation while handling free gas, submersible pumps also require prediction of surging and gas lock conditions. The traditional solutions to those problems are shrouded, and rotary separators to remove free gas ahead of pump inlets. Production rate could also be limited, so that inlet pressure is high enough to avoid damaging vapor-liquid ratios inside pumps. None of these solutions are optimal. Gas separators introduce other limitations and mechanical complications while robbing the system of energy in the form of gas, which lightens fluid density in the tubing just as it does in gas-lift installations. High intake pump pressures have a strong impact on the equilibrium flow rates and the economics of the operation.

Centrifugal pumps will then eventually handle liquid and gas mixtures. A simple way to understand the effect of gas on the pump performance is exemplified by an analysis of the forces acting on gas bubbles dispersed in a continuous liquid phase rotating around an axis. The gas bubbles basically suffer the effect of the forces due to the pressure gradient in the radial direction, and of the drag force which is a function of the difference between liquid and gas radial velocities. The rotating liquid phase centrifugal field causes the force due to the pressure gradient. Since the density of the gas is much smaller than the liquid density, the bubbles under this pressure field would have the tendency of moving towards the lower pressure region closer to the rotational axis.

As a consequence of this interaction, the velocity of the gas becomes smaller than the velocity of the liquid until a point where equilibrium is established between the forces due to the pressure gradient and the slip. The slip velocity causes a change in the void fraction. If the slip is small, the bubbles continue moving under a bubbly flow regime with a void fraction greater than the no slip value. At higher values of slip, the coalescence of the small bubbles at the entrance of the impeller is promoted. Bigger bubbles are more difficult to be carried by the liquid phase and further coalescence of bubbles is induced leading to the formation of a stationary elongated

bubble as was observed by Estevam (2002). At this point a severe degradation in the performance of the pump is experienced. This performance degradation is then explained as a change in the flow pattern, referred as stratified flow by Minemura (1974) or elongated bubble flow by Estevam (2002).

An example of the experimental data obtained in this study is shown in Figure 1. This graph shows a comparison between the experimental data (650 bpd gas flow rate at insitu conditions and 200 psi stage intake pressure), the single-phase performance and the homogeneous model predictions. Results are shown in normalized variables. The normalized pressure increment is the pressure increment divided by the water single-phase shutdown pressure increment. The normalized liquid flowrate is the liquid flowrate divided by the water single-phase flowrate for a null pressure increment.

From the results shown in Figure 1 it can be seen that at a certain in situ gas flow rate, for normalized liquid flow rates higher then 0.7, the balance between the forces due to pressure gradient and slip, results in a normal performance of the pump. Some performance degradation with respect to the homogeneous model prediction is observed due to the fact that the actual gas fraction is bigger than the no-slip value. In this region we can see that as the liquid flow rate decreases, the pressure gradient increases and the slip as a consequence must increase. Consequently bubbly flow regime with higher void fraction is experienced and higher-pressure degradation occurs at smaller liquid flow rates.

At a value of the normalized liquid flowrate of 0.7, the slip becomes so big that the flow becomes unstable, possibly due to the interaction between the bubbles and the formation of a stationary elongated bubble inside the vanes. As a consequence, severe fluctuation is observed and it is said that the pump is surging.

Further reduction of the normalized liquid flowrate beyond 0.6, causes the flow pattern to change to elongated bubble and a severe reduction in the pump performance is observed.

If we continue to decrease the liquid flowrate, the stationary bubble increases in size and for values of the normalized liquid flowrate smaller than 0.2, the stationary bubble occupies almost the totality of the channel and the pump goes into gas lock as was observed by Estevam (2002).

Literature Review

Several studies regarding the ESP performance under two-phase flow condition are available in the literature. Studies both from the Nuclear and Petroleum industries have been fundamental to understand trends and to provide insight on real behavior of ESP's when handling multiphase flow. In the next paragraphs a brief literature review of the most important works from the Petroleum industry will be presented.

Lea and Bearden (1982)

The authors tested three different pumps, the I-42B and C-72 of radial type stages and the K-70, which is of, mixed flow type, using diesel-CO2 as two-phase mixture. Experiments were conducted to observe the behavior of ESP under two-phase flow conditions. This was essentially an experimental work and the authors presented no correlations or models to account for the observations. They concluded that the use of homogeneous model based on the no slip mixture density and mixture total volumetric flow rate may simply not be adequate to describe head performance under two phase flow conditions.

Turpin (1986)

Using the data of Lea and Bearden, Turpin developed empirical correlations to predict the head-capacity curve for the studied pumps as a function of the free gas-liquid ratio, liquid flow rate and pump intake pressure. Two correlations to predict two-phase head performance were achieved. One single correlation for I-42B radial and K-70 mixed type pump and another for C-72 radial pump. These Correlations are pump specific and can predict the head capacity curve fairly well for low gas volumes at low intake pressures and for higher gas volumes at higher suction pressures. The prediction falls off in the direction of higher gas fractions and lower intake pressure conditions, however the region of poor predictive capability of these correlations coincides with the region of unacceptable pump performance. To quantify the region of unacceptable pump performance, a correlation was developed based on an auxiliary parameter ϕ which should be greater than 1 for the pump to have acceptable performance and is defined as:

$$\phi = 2000\left(\frac{VLR}{3P_i}\right) \tag{1}$$

where P_i is the pump intake pressure in psia, and VLR is the vapor liquid ratio which is defined as the ratio of the in situ volume of free gas to the in situ volume of liquid, and expressed as:

$$VLR = \frac{q_g}{q_l} \tag{2}$$

where q_g and q_l are the gas and liquid flow rates at in situ conditions respectively.

Dunbar (1989)

Dunbar presented a general correlation for determining the applicability of homogeneous model in a graphical form. The author relates the maximum gas or vapor liquid ratio where homogeneous model can be applied as a function of stage intake pressure. Dunbar constructed a reference curve called " Dunbar Curve" for minimum intake pressure that should be attained for a given gas liquid ratio, to apply homogeneous

model without head degradation. This is a very important experimental work based on real field data, but unfortunately, it does not provide information on some of the theoretical aspects.

Sachdeva (1989)

The author presented the first two-phase flow model for ESP stages developed in the petroleum industry. His work was an adaptation of the nuclear industry models to the multi-stage pumps used in ESP installations. This work was not experimental in nature but included data from Lea and Bearden (1982) to calibrate the model and to develop a correlation for the two-phase flow head.

Cirilo (1998)

Cirilo measured the performance of three different submersible centrifugal pumps for handling two-phase flow. Two pumps were of mixed flow type (GN4000 and GN7000), and another one was radial type (GN2100). The experimental data were obtained using air and water as working fluids. The effect of number of stages were studied with 6,12 and 18 stages using GN4000 pump. An important contribution of this work was a correlation to determine the maximum free gas fraction for stable operation of tested mixed flow electric submersible pumps.

Romero (1999)

This work evaluated an improved commercial slotted impeller stage design named Advanced Gas Handler (AGH). This device was designed to increase the maximum free gas fraction that electric submersible pumping systems can handle. Cirilo's experimental data for a 12-stage GN4000 pump (mixed flow) was used in order to establish a comparative base scenario with the AGH. Correlations were developed to predict two-phase head performance for the pump GN4000 and the tested Advanced Gas Handler.

Pessoa (2000)

Experiments were conducted at the facility provided at TUALP using Air-Water at 100 psig pump intake pressure keeping gas mass rate constant and varying liquid flow rates. This experimental set up used a pump with 22-stages instrumented to measure pressure increments across each stage. For the first time stage wise two-phase performance were evaluated and presented. Experimental results based on average efficiency of the pump and average brake horsepower consumption was also presented.

Estevam (2002)

A one-dimensional model of the two-phase flow (air-water) inside the impeller and the diffuser of a centrifugal pump were developed. An experimental facility in transparent material was built to observe the phenomena inside the impeller channel. Depending on the operating conditions, an area where a stationary elongated bubble and another area with dispersed bubble flow were observed. A mechanistic model was developed based on dimensionless numbers to describe the performance of the stage under two phase-flow conditions.

Beltur (2003)

The author collected two-phase data, at pump speed of 2916 rpm (50 HZ) and pump intake pressures from 50 psi to 250 psi in steps of 50-psi increments. The author concluded that stage position has an important effect on performance as downstream stages experience better intake conditions, such as higher intake pressure, more homogeneous mixture and smaller gas void fraction than upstream stages. He also observed that with the increase in intake pressure, stage performance improves and the liquid flow rate at which peak performance was observed moves towards lower liquid flow rates, thus improving the range of operable liquid flow rate. With the increase in gas mass flow rate, the stage performance deteriorates and the liquid flow rate at which peak performance is observed moves towards higher liquid flow rates, reducing the range of operable liquid flow rate.

Sun (2003)

This work presented a simple and accurate theoretical model to predict ESP head performance under two-phase flow conditions. The model predicts pressure and void fraction distributions along impellers and diffusers and can also be used to predict the pump head performance curve under different fluid properties, pump intake conditions, and rotational speeds. The new two-phase model was validated with the air-water experimental data from Beltur (2003). Results shown that the model provides a very good prediction for the pump head performance under different gas flow rates, liquid flow rates, and different intake pressures except for very low gas flow rate with low liquid flow rate. Sun's model is also capable of predicting surging and gas lock conditions.

Experimental Research at TUALP

A commercial, 22-stage pump, modified to measure the pressure at each individual stage was used in this work. Temperature transmitters were used to measure temperatures at the inlet and the discharge of the pump. Liquid and gas flow rate were measured using mass flow meters.

In order to study the pressure effects on ESP performance, a differential pressure sensor was installed at the 10th stage. A layout of the facilities setup is shown in Figure 2.

Single Phase Tests

Single-phase tests were conducted at 42 Hz (2450 rpm) with water as the working fluid at stage intake pressures of 100,

150, 200 and 250 psi. Tests were conducted at different pressures to check the repeatability of single-phase performance. A total of 88 points were collected. Single-phase data was used to obtain the normalizing parameters, namely the single phase shut in pressure and the liquid flowrate at null pressure increment for the 10th stage.

Two-Phase Data

Two-phase flow tests were conducted, varying the 10th stage pressure from 50 psi to 350 psi, in steps of 50 psi. Gas mass rates were varied form 5000 scfd to 90000 scfd, and liquid flow rates were varied from 2000 to 6950 bpd, depending upon the intake pressure at which the tests were conducted. Total number of data points collected for two-phase flow conditions was 1162.

Analysis of Two-Phase Data

In the next sections the experimental data collected is analyzed. Discussion on the flow pattern and stage intake pressure on ESP performance is presented.

Flow Patterns

Two distinct regions were observed in the performance of the stage under two-phase flow conditions:

The first region is a region where some mild performance degradation is observed. This region corresponds to the bubbly flow conditions inside the pump channels as described by Estevam (2002).

The second region is the region where the pump suffers a dramatic and severe performance degradation. This region corresponds to the elongated bubble flow regime region as described by Estevam (2002).

Figure 3, shows a clear example of the two defined regions for a constant gas mass rate of 30000 scfd, at stage intake pressures varying from 50 to 350 psi.

An unstable transition region exists between those two flow regimes. In this region severe fluctuation of the test variables was observed during the experiments. The experimental measurements in this region also indicate a drastic change in the measured variables with respect to time. The bubbly flow regime is unstable and the test point moves to the more stable elongated flow regime. This can be seen in Figure 4 that illustrates all the experimental points collected for each test as well as the average values for gas mass flow rate of 50000 scfd and 200 psi of stage intake pressure. For liquid flow rates higher than 5000 bpd the flow regime is bubbly flow and small fluctuations were observed. For liquid flow rates smaller than 4200 bpd the flow regime is elongated bubble flow and small fluctuations were also observed. For liquid flow rates between 4200 and 5000 bpd the flow was unstable with a tendency of the test point to move towards the elongated bubble flow conditions.

According to Estevam (2002), for very small liquid flow rates in the elongated bubble flow regime, the bubble occupies almost the total length of the impeller channel. At this point, the phenomenon called gas lock is initiated, when practically no pressure is generated. Due to restrictions in TUALP experimental facilities to run tests at low liquid flow rates this phenomenon was rarely observed. An example of this condition is shown in Figure 4, for a liquid flow rate of 1300 bpd.

Stage Intake Pressure Effects

The effect of stage intake pressure is of supreme importance on the performance of the stage. The performance of the pump under two-phase flow conditions increases with higher stage intake pressures. Figure 5 shows a clear example of these phenomena for a constant gas mass rate of 30000 scfd. At higher intake pressures, the pressure increment developed by the pump increases and also the transition from bubbly to elongated flow regime moves towards regions of smaller liquid flow rates and higher pressure increments.

This effect can be explained by the effect of pressure on the in situ gas volume and the bubble sizes. The force balance on the bubbles is extremely affected by the bubble size. Smaller bubbles tend to be more easily carried by the liquid phase than larger bubbles, thus allowing the transition between bubbly to elongated flow regime to occur at smaller values of liquid flowrate and higher values of pressure increment for higher values of pressure. The dependence of the in situ gas volumetric flowrate on pressure also helps to explain the higher performance observed in the bubbly flow regime. At higher pressures, the insitu gas volumetric flow rates and the no-slip gas fraction are smaller explaining the better performance observed.

The effect of pressure can also be seen on Figure 6. This graph shows the results for a constant insitu volumetric gas flowrate between 400 and 500 bpd. For a constant gas volumetric flow rate and constant liquid flow rate, the no-slip gas fraction is independent of the pressure. In the bubbly flow regime, the bubbles are already being carried out easily by the liquid phase and no significant effect of pressure is seen on the performance of the pump in this regime based on the in-situ gas volumetric flowrate. However, the effect of pressure is observed only in the transition boundary between bubbly flow and elongated bubble regimes since at that point the bubble size is a crucial variable to determine the equilibrium conditions and the stable spatial arrangement of the phases.

Modeling

This section presents the single phase and the two-phase drift flux models. The drift flux model is the model adapted to describe the performance of the centrifugal pump performance under the bubbly flow regime.

The elongated bubble regime requires a different approach and is going to be addressed in another section where a correlation will be presented based on the experimental data.

Single Phase Modeling

For an infinitesimal control volume, the steady state flow of an single-phase fluid, can be described using the mass and the linear momentum balance equations, which can be written as:

$$\nabla.(\rho \boldsymbol{V}) = 0 \tag{3}$$

$$\nabla.(\rho \boldsymbol{V}\boldsymbol{V}) + \nabla.(P\boldsymbol{\delta_{ij}}) - \nabla.\boldsymbol{\tau_{ij}} - \rho_K \boldsymbol{g} = 0 \tag{4}$$

where ρ is the fluid density, $\boldsymbol{\tau_{ij}}$ represents the components of the viscous shear stress tensor, $\boldsymbol{\delta_{ij}}$ is the Kronecker delta, $\boldsymbol{g}$ is the external body force vector, P is the pressure and $\boldsymbol{V}$ is the fluid velocity vector.

The solution of the set of mass and momentum balance equations to obtain the spatial pressure and velocity fields is a very complex task. Minemura (1974), Sachdeva (1989) and Sun (2003) developed different models to solve this problem. It is known that the exact solution is a function of pump geometry and size, fluid properties (viscosity and density), roughness of channels, rotational speed and flowrate.

For the flow of low viscosity fluids inside certain pump geometry at a constant rotational speed, we can write that the stage pressure increment ΔP is:

$$\Delta P\{\rho, q\} = g\,\rho H\{q\} \tag{5}$$

where q is the flow rate, g is the gravity acceleration ρ is the fluid density and H is the stage head. The stage head is a function of the velocity field, which is a function of the flowrate q. The head H is usually determined experimentally using water.

The Drift Flux Model

The Drift Flux model is also known in the literature as the Diffusion model or the Mixture model. In this model, the two fluids are considered as a mixture and the usual treatment for the mass conservation equations is to have a mixture mass conservation equation and a diffusion equation, usually given in the form of one of the phase's mass conservation equation. This is mathematically equivalent to the use of the mass conservation equations for both phases. The momentum conservation equation on the other hand is written for the mixture. Since a single mixture linear momentum balance equation is used, the interfacial term effects must be obtained through an extra closure equation. This closure equation is usually obtained based on experimental data. The equations for the mass and momentum steady state Drift Flux model are given below.

$$\nabla.(\alpha_k \rho_k V_k) = 0 \tag{6}$$

$$\sum_{k=l,g}\left[\nabla.(\alpha_k \rho_k V_k V_k) + \alpha_k \nabla.P - \alpha_k \nabla.\tau_{ij} - \alpha_k \rho_k g\right] = 0 \tag{7}$$

where k is an index indicator of the gas (g) or the liquid (l) phases and α_k is the phase volumetric fraction. Prediction of the performance of centrifugal pump stages can theoretically be obtained by solution of this set of mass and momentum balance equations with the associated closure equation and proper boundary conditions. This is of much higher complexity than the single-phase case.

Solving Equation 7 for ∇P, we can obtain the following expression:

$$\nabla P = \sum_{k=l,g} -\nabla.(\alpha_k \rho_k \boldsymbol{V}_k \boldsymbol{V}_k) + \alpha_k \nabla.\boldsymbol{\tau}_{ij}^{k} + \alpha_k \rho_k \boldsymbol{g} \tag{8}$$

The objective of this section is to obtain a simplified model for small no-slip gas fractions and small slip values under the bubbly flow regime. For those conditions we can assume that in some cases where the actual gas fraction is different than the no-slip value but it is constant along the channels this equation can be re-written as:

$$\nabla P = \sum_{k=l,g} \alpha_k \left(-\nabla.(\rho_k \boldsymbol{V}_k \boldsymbol{V}_k) + \nabla.\boldsymbol{\tau}_{ij}^{k} + \rho_k \boldsymbol{g}\right) \tag{9}$$

Also assuming that the gas liquid interaction has a small effect on the phases streamlines and assuming that the local slip between liquid and gas is small, this equation can then theoretically be integrated along the pump channel to yield:

$$\Delta P = (1-\alpha)\Delta P\left\{\rho_l, q_L^*\right\} + \alpha\,\Delta p\left\{\rho_g, q_g^*\right\} \tag{10}$$

Where q_l^* and q_g^* respectively are the liquid and gas flow rates corresponding to the actual liquid and gas velocities fields under two-phase flow conditions, and α is the slip gas void fraction. Substitution of Equation 5 into Equation 10 yields:

$$\Delta P = (1-\alpha)\rho_l H\left\{q_l^*\right\} + \alpha\rho_g H\left\{q_g^*\right\} \tag{11}$$

Since the gas fraction is assumed constant along the channels we can calculate the values of q_l^* and q_g^* respectively as:

$$q_l^* = \frac{q_l}{(1-\alpha)} \tag{12}$$

$$q_g^* = \frac{q_g}{\alpha} \tag{13}$$

where q_l and q_g are the in-situ liquid and gas volumetric flow rates at stage intake conditions. Then, the final pressure increment equation can be expressed as:

$$\Delta P = (1-\alpha)\rho_l H\left\{\frac{q_l}{(1-\alpha)}\right\} + \alpha\rho_g H\left\{\frac{q_g}{\alpha}\right\} \tag{14}$$

The applicability of this simplified model should be restricted to small values of no-slip gas fractions under conditions of small slip between the phases. Under those conditions, the bubbles continue moving under bubbly flow regime, with small disturbance to the liquid phase and this model should provide a reasonable approximation for the behavior of the pump. At higher values of slip, the gas void fractions increases, the coalescence of the small bubbles at the entrance of the impeller is promoted, leading to the formation of a stationary elongated bubble (Estevam 2002), then a severe degradation in the performance of the pump is experienced, and the described model is not valid any longer.

Since one momentum equation has been eliminated from the system, the relative motion of the phases should be expressed by an additional closure relationship. This is usually done by providing a correlation to calculate the slip velocity or the slip gas void fraction.

A Special Case – The Homogeneous Model

A commonly used method for predicting the two-phase performance of an ESP pump is based on the homogeneous model. In this model, the two-phase mixture is assumed to behave as a homogeneous fluid. The homogeneous model is a special case of the model given by Equation 14.

Under no-slip conditions we can write that the slip gas fraction is equal to the no-slip gas fraction.

$$\alpha = \lambda \tag{15}$$

And the mixture flow rate q_m can be calculated as:

$$q_m = q_l + q_g \tag{16}$$

Under this assumption it is possible to write that:

$$\frac{q_l}{1-\alpha} = \frac{q_l}{1-\lambda} = \frac{q_g}{\alpha} = \frac{q_g}{\lambda} = q_m \tag{17}$$

Replacing Equation17 into Equation 14, it is possible to obtain an expression for the homogeneous model pressure increment as:

$$\Delta P = g\rho_m H\{q_m\} \tag{18}$$

where ρ_m is the mixture density which can be calculated by:

$$\rho_m = \rho_l(1-\lambda) + \rho_g\lambda \tag{19}$$

Figures 7 and 8 shows the results of the homogeneous model pressure increment predictions at low gas in situ volumetric flow rate (100-200 bpd) and at high gas in situ volumetric flow rate (900-1000 bpd). As it can be observed, the homogeneous model predicts well for low gas flow rates or when the actual slip inside the channels is small. It never does a good prediction on the transition boundary or elongated bubble regime.

Figures 9 and 10 shows the comparison of the pressure increment calculated with the homogeneous model versus the experimental pressure increment for each flow regime. The calculated absolute average error for the pressure increment using the homogeneous model for bubbly flow is 0.615 psi, and the absolute average error for the pressure increment using the homogeneous model for elongated bubble flow is 5.690 psi.

Bubbly Flow Regime Model Closure Correlation

In order to close the drift flux model for the bubbly flow regime, a closure equation for the gas fraction is required. The drift flux model Equation 14 was used to calculate the value of gas slip fraction, since all other experimental values in this equation are known.

Figure 11 shows the relationship between the normalized in-situ gas and liquid flow rates for each value of the mixture density.

Based on these experimental results, the following correlation is proposed:

$$q_g = \left(a\frac{\rho_m}{\rho_l} + b\right) * (q_l)^c \tag{20}$$

Where q_L and q_g are the normalized liquid gas flow rates at in situ conditions, ρ_m and ρ_l are the mixture and liquid density, and a, b, c are constant values equal to:

$$a = -0.843$$
$$b = 0.850$$
$$c = 1.622$$

This concludes the closure of the model. For a certain known value of liquid and gas flow rates at in situ conditions one can use Equation 20 to calculate the value of the mixture density, which can then be used to solve Equation 19 for the actual gas fraction. Finally the value of the gas fraction is used in the model Equation 14 to calculate the model pressure increment.

Figures 12 and 13 shows the results of the proposed model to calculate the pressure increment at low gas (100-200 bpd) and

at high gas (900-1000 bpd) in situ volumetric flow rates, as well as the predictions from the homogeneous model.

Figure 14 shows the comparison of the pressure increment calculated with the proposed model versus the experimental pressure increment for bubbly flow regime. The calculated absolute average error for the pressure increment using the new correlation for bubbly flow is 0.199 psi, while for the homogeneous model is 0.615 psi. This represents a significant improvement on the accuracy predictions for the bubbly flow regime region.

Surging Prediction

The transition region is defined by two boundaries. The first one is the boundary where the bubbly flow regime becomes unstable and the other one is where the elongated bubble regime is established.

A pressure effect was observed on the bubbly flow instability boundary however in the elongated bubble regime boundary the pressure effect was not observed.

Unstable Bubbly Flow

Figure 15 shows the relationship between the normalized gas and liquid in-situ volumetric flowrates and the gas density for the unstable bubbly flow regime boundary.

The following correlation is proposed to describe this relationship:

$$q_g = \left(a\frac{\rho_g}{\rho_l} + b \right) * \left(q_l \right)^c \tag{21}$$

Where q_l and q_g are the normalized liquid gas flow rates at in situ conditions, ρ_g and ρ_l are the gas and liquid densities, and a, b, c are constant values calculated to minimize the error and equal to:

$$a = 5.580$$
$$b = 0.098$$
$$c = 1.421$$

The results of these surging criteria expressed in terms of pressure increment, liquid flow rate as a function of the stage intake pressure can be observed in a graphical form in Figure 16.

Stable Elongated Bubble Flow

Figure 17 shows the relationship between the gas and liquid in-situ volumetric flow rates for the conditions where the elongated bubble is formed.

The following correlation is proposed to represent this relationship:

$$q_l = a * q_g^b \tag{22}$$

Where q_l and q_g are the normalized liquid gas flow rates at in situ conditions, and a, b, are constant values calculated by regression and equal to:

$$a = 1.6213$$
$$b = 0.435$$

The results of these transition criteria expressed in terms of pressure increment, liquid flow rate can be observed in a graphical form in Figure 18.

Elongated Bubble Flow Correlation

The drift flux model cannot be extended to the elongated bubble flow regime. A correlation is then proposed to calculate the pressure increment for those conditions. Figure 19 shows the experimental values of the pressure increment as a function of the in-situ gas volumetric flowrate for the elongated bubble region.

The following correlation is proposed to for the normalized pressure increment:

$$\Delta P = a + b * \ln(q_g) \tag{23}$$

Where q_g is the normalized gas flow rates at in situ conditions, and a, b, are constant values calculated by regression and are equal to:

$$a = -0.47075$$
$$b = -0.21626$$

Figure 20 and 21 shows the comparison of the results obtained to calculate the pressure increment using the procedure described before with the experimental pressure increment data in the elongated bubble flow region at low (100-200 bpd) and high (900-1500 bpd) gas in-situ volumetric flow rates. It can be observed in these graphs that very good results were obtained. That figures also shows the results from the homogeneous model.

Figure 22 shows the comparison of the pressure increment calculated with the proposed model versus the experimental pressure increment for the elongated bubble flow regime. The calculated absolute average error for the pressure increment using this correlation is 0.172 psi while for the homogeneous model is 5.690 psi, under elongated bubble flow conditions. This is a remarkable improvement in the prediction accuracy for the elongated bubble flow regime.

Final Results

Figures 23 to 27 show the results of the proposed bubbly flow model and the elongated bubble flow correlation for gas in situ flow rates of 100-200, 400-500, 600-700, 800-900, 1000-1500 bpd. Those pictures also show the prediction based on the homogenous model. As can be seen for all experimental results the proposed bubby flow model and elongated bubble regime correlation outperform the prediction from the homogeneous model.

Conclusions

1. The presence of free gas affects the performance of centrifugal pumps, these effects may vary from slight interference to gas locking.

2. The acquired experimental data supports the existence of three flow regimes inside the stage of an electric submersible pump: One with standard performance of centrifugal pumps in single-phase, where the pressure increment is increasing when decreasing the liquid flow rate. The second region is the elongated bubble regime where severe degradation of performance is observed. The region in between those two flow regimes is unstable.

3. When the phenomenon of transition occurs, as the fluid flow rate is reduced, a reduction of the head or pressure increment is observed. The experimental measures in this region also indicate a fluctuation in the measured values of the pressure increment with respect to time. It is valid to affirm that the points recorded in this transition region does not exists, they only correspond to the average of the values recorded during the period of fluctuation when the flow pattern is changing from bubbly flow to elongated bubble flow regime.

4. Experimental results show a negligible effect of the stage intake pressure on the pressure increment developed by the stage for a constant liquid flow rate and constant gas volumetric in situ flow rate. The effect of pressure is observed only in the boundary of the bubbly flow regime as a displacement of the point of peak performance as the stage intake pressure is increased. The maximum stage intake pressure tested was around 350 psi and at this level the most significant effect of pressure is over the in-situ gas volumetric fraction and bubble sizes. At higher pressure levels it is expected that a secondary effect related to the difference between the gas and liquid densities will promote a better pump performance.

5. Correlations to determine the pressure increment under bubbly flow and elongated bubble flow conditions were developed, and also transition criteria from bubbly to transition flow and also from elongated bubble to transition flow.

6. Better results were obtained using these new correlations, in comparison with the results obtained using the homogeneous model, getting a notorious improvement specially in the elongated bubble flow region.

7. Results presented in this work are only valid for air-water mixtures. They serve as a worst case scenario for real applications using real oil and natural gas.

Acknowledgements

The progress on this work is the direct result of the technical and financial support of Tulsa University Artificial Lift Projects' member companies: ENI-AGIP, CENTRILIFT, PDVSA, PEMEX, ONGC, SCHLUMBERGER, SHELL, PETROBRAS and TOTALFINAELF.

Nomenclature

$\{\ \}$	Function
a,b,c	Constants
g	Gravitational constant
H	Head
P	Pressure
q	Flow rate
q^*	Equivalent Flow rate
V	Velocity
VLR	Vapor Liquid Ratio
ΔP	Pressure increment
λ_g	No slip void fraction
α	Phase fraction
ρ	Density
ϕ	Turpin auxiliary parameter
δ_{ij}	Kronecker delta
τ_{ij}	Viscous shear stress tensor

Subscripts/ Superscripts

m	Mixture
l	Liquid
g	Gas
i	Intake

References

1. Estevam, V.: "*Uma Análise Fenomenológica da Operação de Bomba Centrífuga com Escoamento Bifásico*," Ph.D Thesis, Universidade Estadual de Campinas (2002).
2. Beltur, R.: "*Experimental Investigation of Two-Phase Flow Performance Of Electrical Submersible Pump Stages*," MS Thesis, The University of Tulsa (2003).
3. Duran, J.: "Pressure Effects on ESP Air-Water Performance," MS Thesis, The University of Tulsa (2003).
4. Cirilo, R.: *Air-Water Flow Through Electric Submersible Pumps*, MS Thesis. The University of Tulsa, Oklahoma (1998).

5. Dunbar, C.E.: "*Determination of Proper Type of Gas Separator*," Microcomputer Applications in Artificial Lift Workshop. SPE Los Angeles Basin Section (October 15-17. 1989).
6. Lea, J.F. and Bearden, J.L: "Effect of Gaseous Fluids on Submersible Pump Performance," paper SPE 9218 published in the *JPT* (December 1982) pp 2922-2930
7. Pessoa, R.: " Experimental Investigation of Two-Phase Flow Performance Of Electrical Submersible Pump Stages," MS Thesis, The University of Tulsa (2000).
8. Romero, M.: *An Evaluation of an Electric Submersible Pumping System for High GOR Wells*, MS Thesis, The University of Tulsa, Tulsa, Oklahoma (1999).
9. Sachdeva, R.: *Two-Phase Flow Through Electric Submersible Pumps*, MS Thesis. The University of Tulsa, Oklahoma (November 1998).
10. Turpin, J.L., Lea, J.F. and Bearden, J.L.: "Gas-Liquid Flow Through Centrifugal Pumps-Correlation of Data," 3rd Int'l Pump Symposium, Texas A&M University (May 1986).
11. Sun, D.: "*Modeling Gas-Liquid Head Performance Of Electrical Submersible Pumps*," PhD Thesis Dissertation, The University of Tulsa (2003).
12. Pessoa, R, Sun, D. and Prado, M.: "State of the Art: Experimental Work on ESP Performance under Two-Phase Flow Conditions", TUALP ABM. Tulsa, OK November 17, 2000
13. Kallas, P and Way K.: "An Electrical Submersible Pumping System for High GOR Wells," SPE Electrical submersible pump workshop, April 26-28, 1995
14. Wilson, D.G et al.: "Analytical Models and Experimental Studies of Centrifugal Pump Performance in TEO Flow,' MIT Research project 493, NP –677, (1979), prepared for EPRI
15. Wilson, B.L.: "Gas handling centrifugal Pumps," SPE Electrical Submersible Pump Workshop, (1998).

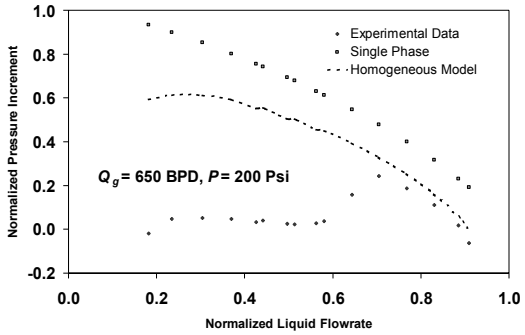

Figure 1: Comparison of Homogeneous Models with Actual Performance for Stage 10.

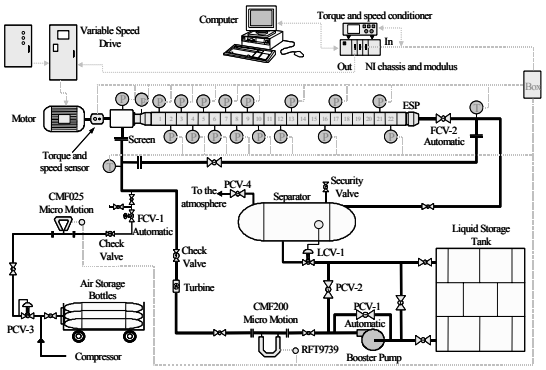

Figure 2: TUALP Facilities Layout

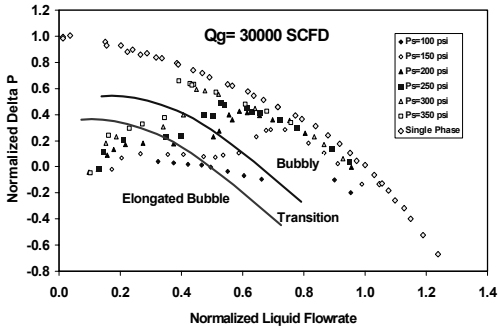

Figure 3 –Two-Phase Flow Performance

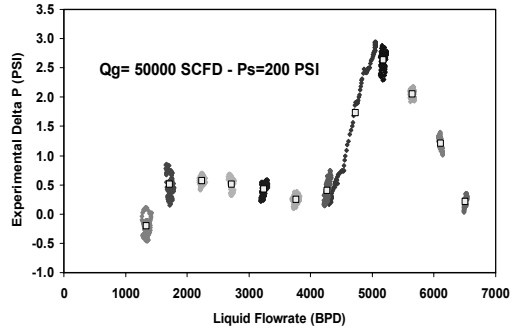

Figure 4 – Fluctuation of the Data According to the Flow Pattern.

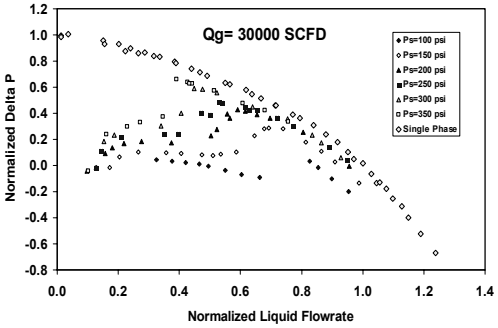

Figure 5 – Two-Phase Performance of the Stage at Different Intake Pressure

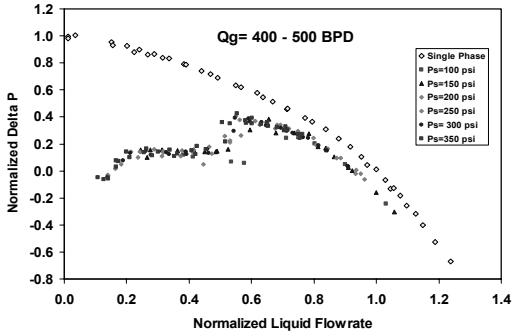

Figure 6 – Two-Phase Performance of the Stage at Different Intake Pressure

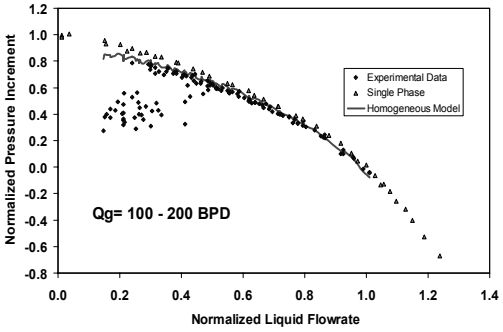

Figure 7 – Homogenous Model Performance

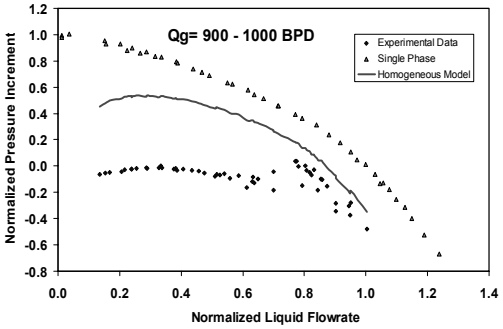

Figure 8 – Homogenous Model Performance

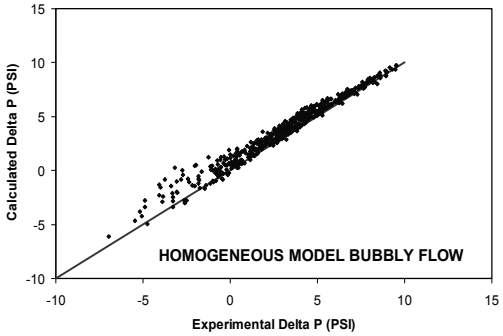

Figure 9 – Homogenous Model Performance in Bubbly Flow Regime

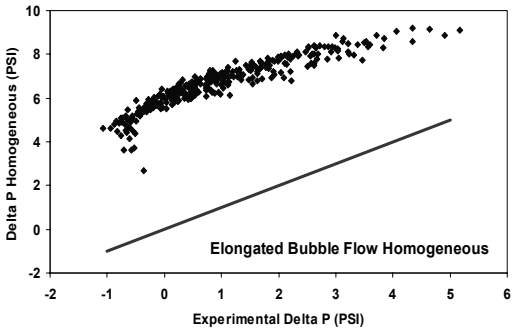

Figure 10 – Homogenous Model Performance in Elongated Bubble Flow Regime

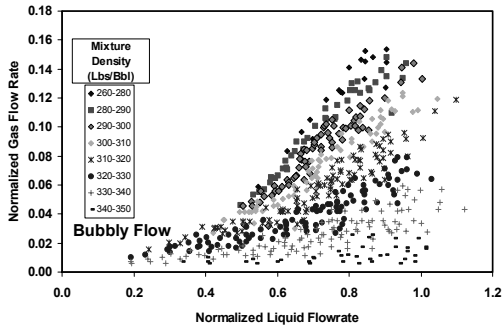

Figure 11 – Experimental Bubbly Flow Regime Data

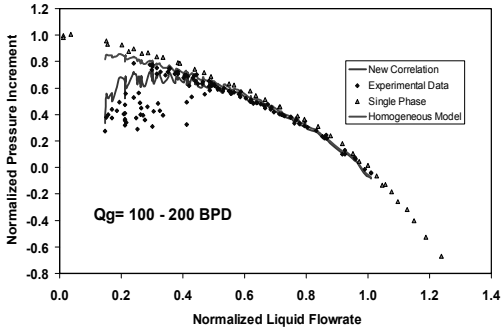

Figure 12 – Performance of the Bubbly Flow Correlation

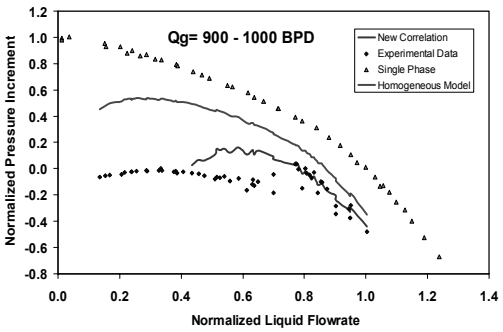

Figure 13 – Performance of the Bubbly Flow Correlation

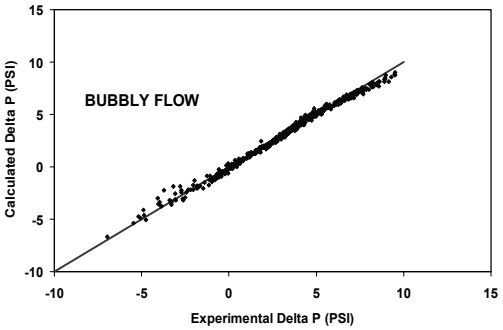

Figure 14 –Bubbly Flow Model Performance

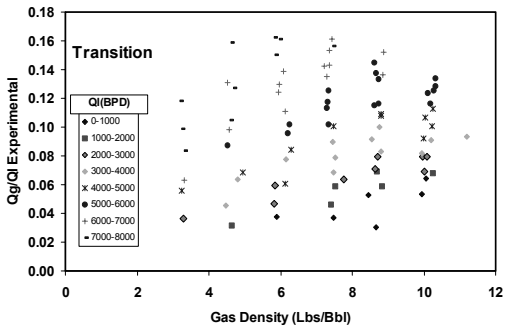

Figure 15 – Experimental Values Used to Develop the Correlation for Surging Criteria

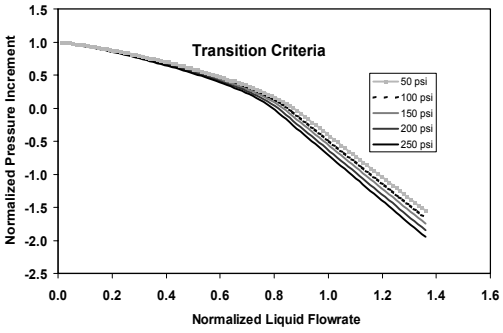

Figure 16 – Normalized Surging Criteria

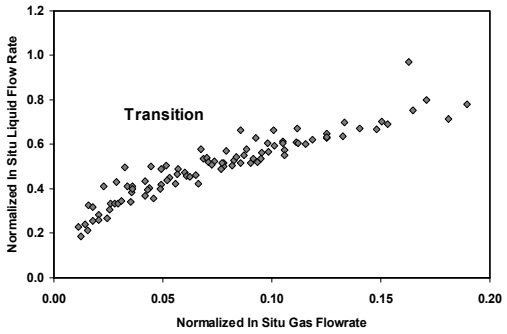

Figure 17 – Elongated Bubble Transition Data

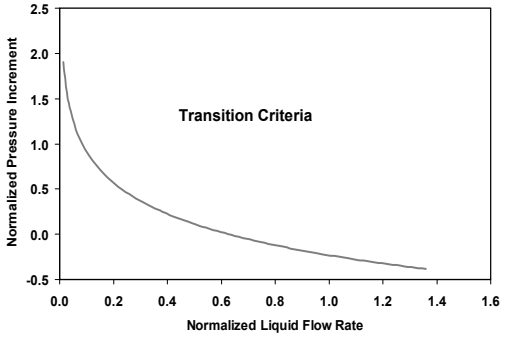

Figure 18 – Elongated Bubble Transition Criteria

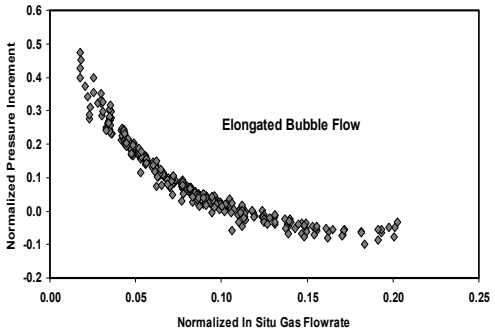

Figure 19 –Elongated Bubble Regime Data

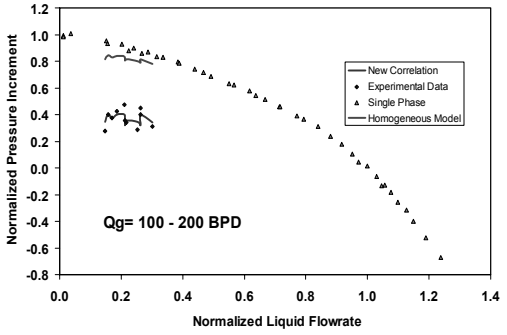

Figure 20 –Results of the New Correlation for Elongated Bubble Flow

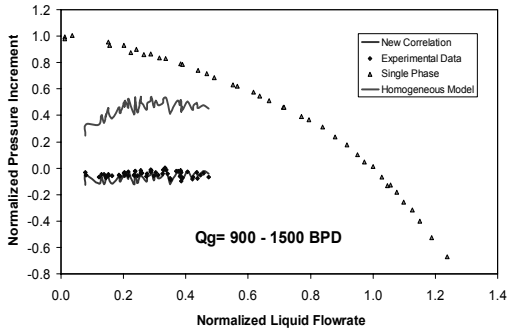

Figure 21 –Results of the New Correlation for Elongated Bubble Flow

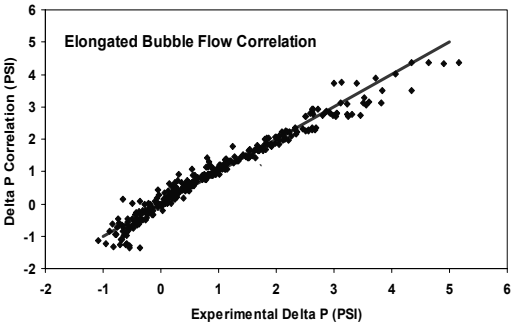

Figure 22 –Elongate Bubble Correlation Performance

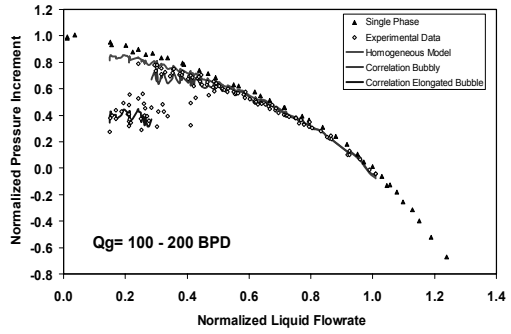

Figure 23 – New Model and Correlations Results

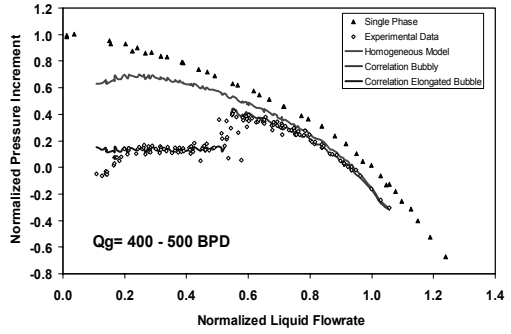

Figure 24 – New Model and Correlations Results

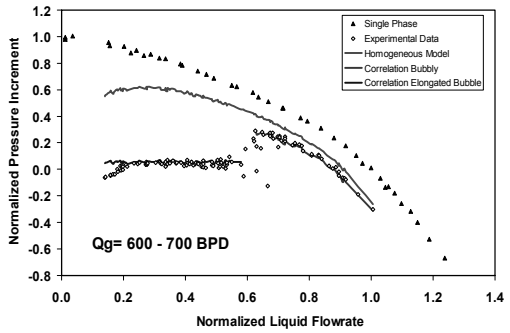

Figure 25 – New Model and Correlations Results

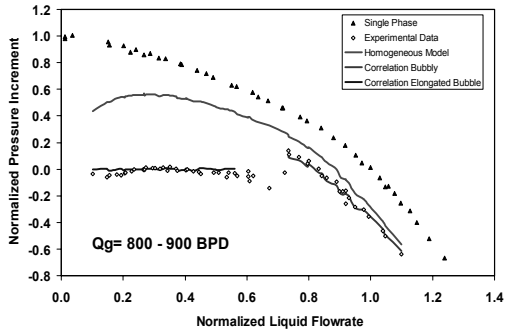

Figure 26 – New Model and Correlations Results

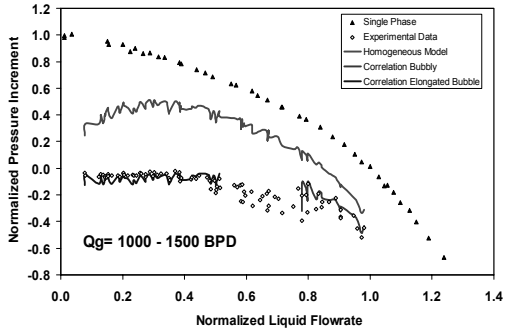

Figure 27 – New Model and Correlations Results